Radboud Repository

Radboud University Nijmegen

PDF hosted at the Radboud Repository of the Radboud University Nijmegen

The following full text is a publisher's version.

For additional information about this publication click this link.
http://hdl.handle.net/2066/198331

Please be advised that this information was generated on 2021-07-19 and may be subject to change.

Rapid Communications

Non-Heisenberg covalent magnetism in iron oxide clusters

R. Logemann,[1] A. N. Rudenko,[2,1,3] M. I. Katsnelson,[1] and A. Kirilyuk[1,4,*]

[1]*Radboud University, Institute for Molecules and Materials, Heyendaalseweg 135, 6525 AJ Nijmegen, The Netherlands*

[2]*School of Physics and Technology, Wuhan University, Wuhan 430072, China*

[3]*Theoretical Physics and Applied Mathematics Department, Ural Federal University, 620002 Ekaterinburg, Russia*

[4]*FELIX Laboratory, Radboud University, Toernooiveld 7c, 6525 ED Nijmegen, The Netherlands*

(Received 19 April 2018; published 16 July 2018)

The sensitivity of material properties to the atomic and nanoscale morphology is most clearly demonstrated in small gas-phase clusters. In particular, magnetism serves as an extremely sensitive probe of the smallest modifications of atomic environment. This Rapid Communication demonstrates the drastic changes in both the exchange mechanism and the atomic moments in iron oxide clusters as compared to the bulk. In particular, the exchange is essentially non-Heisenberg and the exchange interactions are increased by an order of magnitude compared to bulk hematite. In addition, very large atomic magnetic moments are observed on oxygen sites due to strong spin polarization. As $Fe_3O_4^+$ and $Fe_5O_7^+$ are pure trivalent, double exchange is excluded and super exchange is the dominant exchange mechanism in these iron oxide clusters. Therefore, the non-Heisenberg behavior is attributed to covalent magnetism as the hybridization between Fe 3*d* and O 2*p* orbitals for clusters is strongly enhanced compared to bulk hematite and becomes magnetic state dependent.

DOI: 10.1103/PhysRevMaterials.2.073001

For the past decades, the demand for further miniaturization of magnetic storage and sensors increased tremendously. Such continuous downscaling trends heavily depend on better understanding of electronic and magnetic properties at the atomic scale. In magnetism, the Heisenberg model for exchange interaction is currently the default model to describe both static and dynamic magnetic properties. Therefore, fundamental knowledge on the applicability of such a model is of utmost importance. Surprisingly, we will show that the Heisenberg model can even fail in classical localized superexchange systems at the atomic scale.

Atomic clusters, with a typical size of 2–20 atoms, are well known for their extraordinary behavior of physical properties as a function of size. For example in magnetism, Rh clusters are magnetic in contrast to nonmagnetic bulk Rh [1,2]. In contrast to paramagnetic bulk phases of Mn, manganese clusters show nonzero magnetic moments with clear oscillations as a function of size [3]. In addition, the magnetic moments of Fe, Co, Ni clusters are enhanced compared to the bulk [4–7]. However, not only the magnetic moments vary as a function of size. In Tb clusters, the exchange interaction strength drastically increases compared to that of the bulk and shows irregular oscillations as a function of the interatomic distances [8].

The Heisenberg exchange model is the most used one to describe the behavior of magnetic systems. Its basic assumptions, namely localized magnetic moment with fixed magnitude and interaction strengths which are independent on the magnetic configuration considered, appear strongly restrictive. Nevertheless, the Heisenberg model is successfully used for a wide range of physical bulk systems such as spin wave excitations in metals [9] and the description of magnetic interactions in transition metal oxides [10–14]. Moreover, also for finite systems such as molecular magnets [15,16], atomic chains [17,18], or clusters on a surface [19], the Heisenberg model has been used successfully.

In this Rapid Communication, we study the mechanisms of exchange interaction, in particular the applicability of the Heisenberg model in iron oxide clusters. Recent determination of their structures [20] form a solid basis for this study. We show that the exchange interactions in clusters drastically depend on the magnetic configuration considered, resulting in strong non-Heisenberg behavior. In particular, for the clusters $Fe_3O_4^+$ and $Fe_5O_7^+$, we exclude the double exchange mechanism and attribute the non-Heisenberg effects to covalent magnetism and unusually strong oxygen spin polarization that unlike in bulk oxides [21] is also present in the ground state.

In transition metal oxides, direct overlap between the 3*d* orbitals is often negligible and indirect exchange mechanisms like superexchange and double exchange are responsible for the magnetic interactions. Superexchange, based on the (virtual) hopping via O *p* orbitals between two sites with equal valence, can be expressed as an effective exchange interaction in the Heisenberg model [22]. In contrast, double exchange, involving two states with different valence, is often associated with non-Heisenberg behavior [23,24].

We first solve the electronic structure at the density functional theory (DFT) level using the hybrid B3LYP exchange-correlation functional [25,26]. For the DFT calculations we used the Vienna *ab initio* simulation package (VASP) [27] using the projector augmented wave (PAW) method [28,29]. A single *k* point (Γ) and an energy cutoff of 400 eV has been used in the calculations. Previously, the geometric structures of $Fe_xO_y^{+/0}$ clusters were studied combining DFT with a genetic algorithm and the cation clusters were verified using infrared multiphoton dissociation spectroscopy [20].

*a.kirilyuk@science.ru.nl

 ©2018 American Physical Society

TABLE I. Magnetic moments of the clusters $Fe_3O_4^+$, Fe_3O_4, and $Fe_5O_7^+$ for both the FiM and FM configurations in μ_B, calculated by Eq. (2) in their magnetic ground state geometry.

	$Fe_3O_4^+$		$Fe_5O_7^+$	
Atom	FiM	FM	FiM	FM
Fe_1	−3.84	3.89	3.84	3.93
Fe_2	3.87	3.90	3.85	3.97
Fe_3	3.87	3.90	3.87	3.97
Fe_4			−3.81	3.93
Fe_5			−3.78	3.97
O_1	0.85	0.86	0.01	0.75
O_2	−0.01	0.86	0.17	0.76
O_3	−0.01	0.86	0.03	0.82
O_4	0.28	0.75	0.74	0.77
O_5			−0.16	0.76
O_6			0.08	0.77
O_7			0.16	0.58

To obtain a localized basis, we map our DFT Hamiltonian onto the basis of cubic harmonics represented by Wannier functions (WF). To this end, the WANNIER90 code is employed [30]. We use five d orbitals for the TM atoms and three p orbitals for oxygen. The resulting tight-binding Hamiltonian has the form,

$$H^\sigma = \sum_i \varepsilon_i^\sigma n_i^\sigma + \sum_{i\neq j} t_{ij}^\sigma c_i^{\sigma\dagger} c_j^\sigma, \tag{1}$$

where σ labels spin up and down, ε_i^σ is the energy of the ith WF and n_i^σ its occupation number. t_{ij}^σ is the hopping parameter between the ith and jth WF and $c_i^{\sigma\dagger}$ (c_j^σ) the creation (annihilation) operator of electrons localized on the ith (jth) WF. The local magnetic moment (M_i) can be obtained from the density of states (DOS) $g_i^\sigma(\varepsilon)$ projected onto the ith WF:

$$M_i = \int_{-\infty}^{E_F} d\varepsilon [g_i^\uparrow(\varepsilon) - g_i^\downarrow(\varepsilon)]. \tag{2}$$

Table I shows the magnetic moments for the clusters $Fe_3O_4^+$ and $Fe_5O_7^+$ for the ferrimagnetic (FiM) and ferromagnetic (FM) configurations. Note that for all studied clusters except neutral Fe_3O_4 the FiM configuration represents the lowest energy state. The magnetic moments according to Eq. (2) of all other considered cluster sizes can be found in the Supplemental Material [31]. In general, $Fe_xO_y^{0/+}$ clusters contain both divalent and trivalent Fe atoms [20]. However, for $Fe_3O_4^+$ and $Fe_5O_7^+$ all Fe are trivalent and have a magnetic moment in the range of 3.8 to 4.0 μ_B.

Whereas the size of the Fe moments is independent between the FiM and FM configurations, the O atoms show unusually strong spin polarization. This spin polarization is determined by the magnetic orientation of the surrounding Fe atoms. In $Fe_3O_4^+$, the atoms O_2 and O_3 are nonmagnetic in the FiM configuration due to the opposite magnetic moments of the two Fe nearest neighbors. In the FM configuration O_2 and O_3 are strongly spin polarized (M = 0.86 μ_B). Note that O_1 is already strongly spin polarized in the FiM ground state configuration. This appearance of spin polarization in the magnetic ground state results from the ferromagnetic alignment between its nearest neighbors Fe_2 and Fe_3. O_4 is special with its location above the center and is bonded to all Fe atoms, resulting in partial spin polarization.

In the FiM ground state of $Fe_5O_7^+$, O_4 has parallel alignment with its nearest neighbors and is therefore strongly spin polarized with 0.74 μ_B. In contrast, for the FM configuration all O in $Fe_5O_7^+$ are strongly spin polarized between 0.6 and 0.8 μ_B. Although the spin polarization in FM $Fe_5O_7^+$ is still strong, on average the spin polarization is reduced with 0.1 μ_B compared to FM $Fe_3O_4^+$.

For comparison, the magnetic moments in bulk hematite using the same method are 4.09 and 4.20 μ_B for Fe in the AFM and FM configuration, respectively [21]. Thus in clusters the Fe moments are 0.2 μ_B lower compared to hematite. In the ground state of hematite, spin polarization of the oxygen sites is negligible ($\leqslant 0.6 \times 10^{-3}$ μ_B). In contrast, here we observe magnetic moments of more than 0.8 μ_B. Even in the fully saturated FM configuration in hematite the oxygen magnetic moment is twice smaller compared to the one in the ground state of $Fe_3O_4^+$ and $Fe_5O_7^+$ clusters.

To calculate the magnetic interactions, we consider the mapping onto the classical Heisenberg Hamiltonian:

$$H = -\sum_{i>j} 2J_{ij}\mathbf{s}_i \cdot \mathbf{s}_j, \tag{3}$$

where $\mathbf{s}_i$ ($\mathbf{s}_j$) is the unit vector in the direction of the magnetic moment on site i (j). J_{ij} is the corresponding exchange interaction between site i and j.

In principle, exchange interactions can be calculated by consideration of multiple magnetic configurations and mapping of the corresponding energy differences onto Eq. (3). For $(Fe_2O_3)_n$ (n = 1–5) such mapping has been achieved and predominantly strong AFM exchange interactions were obtained [32]. However, this method *a priori* assumes the Heisenberg model and is unsuitable to determine any spin-spin angle dependence of the exchange interactions in the system and therefore the applicability of the Heisenberg model in general. Using the magnetic force theorem (MFT) the exchange interactions can be calculated via the second order variations in total energy with respect to infinite small rotations of the magnetic moments for a given magnetic configuration [33]. Multiple magnetic configurations can be used and the applicability of the Heisenberg model can be tested. The MFT based on Wannier orbitals has been successfully used on a variety of systems [13,21,34–38]. In the MFT method, the exchange interactions can be written in the following form [33]:

$$J_{ij} = \frac{1}{4\pi}\int_{-\infty}^{E_F} d\varepsilon \sum_{\substack{m,m'\\ m'',m'''}} \mathrm{Im}\left[\Delta_i^{mm'} G_{ij\downarrow}^{m'm''}(\varepsilon)\Delta_j^{m''m'''} G_{ji\uparrow}^{m'''m}(\varepsilon)\right], \tag{4}$$

where $\Delta_i^{mm'} = \int_{BZ}[H_{ii,\uparrow}^{mm'}(\mathbf{k}) - H_{ii,\downarrow}^{mm'}(\mathbf{k})]d\mathbf{k}$ is the exchange splitting and $G_{ij\downarrow}^{mm'}(\varepsilon)$ is the real-space Green's function that is calculated in reciprocal space by:

$$G_{\mathbf{k}}^\sigma(\varepsilon) = [\varepsilon - H^\sigma(\mathbf{k}) + i\eta]^{-1}, \tag{5}$$

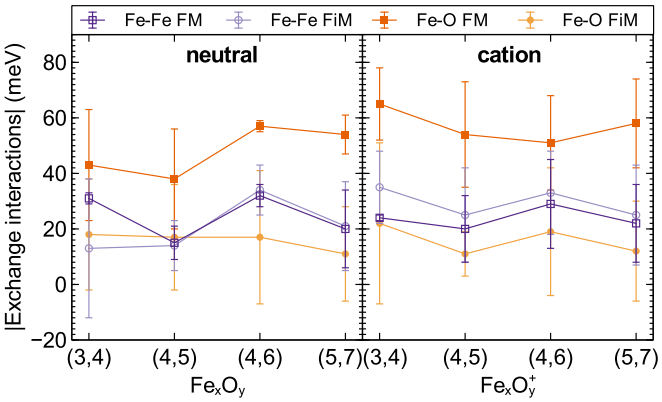

FIG. 1. The absolute value of the average exchange interactions as a function of cluster size (x, y) for the neutral and cation $Fe_xO_y^{+/0}$ clusters. All average Fe-Fe interactions are negative; all average Fe-O are positive.

TABLE II. Exchange interactions of $Fe_3O_4^+$ for the FiM and FM configurations. J and J′ are Fe-Fe and Fe-O exchange interactions, respectively. $J^{\text{eff}}_{\text{Fe1}-\text{Fe2}}$ and $J^{\text{eff}}_{\text{Fe2}-\text{Fe3}}$ are the exchange interactions in the effective Fe model. All exchange interactions can be identified using Fig. 2.

	FiM (meV)	FM (meV)
$J_{\text{Fe1}-\text{Fe2}}$	− 42.3	− 24.6
$J_{\text{Fe2}-\text{Fe3}}$	− 20.6	− 22.1
$J'_{\text{Fe2}-\text{O1}}$	70.1	72.3
$J'_{\text{Fe3}-\text{O4}}$	23.8	48.2
$J'_{\text{Fe1}-\text{O4}}$	4.9	46.1
$J'_{\text{Fe1}-\text{O2}}$	4.0	74.8
$J'_{\text{Fe2}-\text{O3}}$	− 2.6	73.1
$J^{\text{eff}}_{\text{Fe1}-\text{Fe2}}$	− 40.6	54.1
$J^{\text{eff}}_{\text{Fe2}-\text{Fe3}}$	99.8	55.7

where we used $\eta = 0.001$ eV, and $H^{\sigma}(\mathbf{k})$ is the reciprocal Hamiltonian whose elements are obtained from the DFT calculations. The exchange integral calculations are done with an in-house developed code [39].

The mapping of the electronic Hamiltonian onto the Heisenberg model is not uniquely defined due to the strong spin polarization on oxygen, and two options exist to construct the Heisenberg model. In the first model, based on the Anderson principle only exchange interactions between the Fe sites are considered, whereas oxygen atoms only mediate the magnetic interactions via superexchange and/or double exchange. In the second model, oxygen is also considered to be a magnetic center provided it is sufficiently spin polarized. Consequently, additional exchange interactions between Fe and O occur. These Fe-O exchange interactions can be mapped onto an effective model with only Fe-Fe exchange interactions. Both models were systematically evaluated and compared for prototype bulk transition metal (TM) oxides such as NiO, MnO, and hematite [21]. Because in clusters oxygen spin polarization already occurs in the magnetic ground state, we have to include the Fe-O interactions and spin polarization effects into the magnetic Hamiltonian.

Figure 1 shows the absolute value of the average exchange interactions in clusters for both neutral and cation Fe_xO_y clusters as a function of size for both the FiM and FM configuration. The error bars indicate the standard deviation around the average value. All average Fe-Fe exchange interactions are negative and favor AFM alignment, whereas all Fe-O interactions are positive. The difference in average Fe-Fe exchange interactions between the FM and FiM configurations decreases as a function of cluster size, for both neutrals and cations.

Figure 1 clearly shows $Fe_xO_y^{+/0}$ clusters show significant non-Heisenberg behavior, in particular due to the large magnetic moment on the O atoms and the strong dependence on the magnetic configuration considered for the Fe-O interactions.

To understand the origin of the non-Heisenberg behavior in clusters, we highlight the $Fe_3O_4^+$ and $Fe_5O_7^+$ clusters. The individual exchange interactions of $Fe_3O_4^+$ are shown in Table II and can be identified using Fig. 2 where J and J′ correspond to Fe-Fe and Fe-O exchange interactions, respectively. The individual exchange interactions of the other cluster sizes can be found in the Supplemental Material [31]. Note that no O-O exchange interactions are present within the calculated clusters. Therefore, we map the Fe-O exchange interactions onto an effective model with only Fe-Fe exchange interactions using [21]:

$$J_{ij}^{\text{eff}} = J_{ij} + \frac{\sum_k J'_{ik} J'_{kj}}{|\sum_l J'_{li}|} + \frac{\sum_k J'_{ik} J'_{kj}}{|\sum_l J'_{lj}|}, \tag{6}$$

where i and j (k and l) label Fe (O) sites, respectively. J'_{ik} is the Fe-O exchange interaction between Fe site i and O site k.

As is shown in Table II, the effective exchange interactions heavily depend on the local magnetic configuration. In the FiM configuration, the effective exchange interactions differ by a factor of two and have an opposite sign despite the fact that their local geometric structure is very similar. In the FM configuration $J^{\text{eff}}_{\text{Fe1}-\text{Fe2}}$ and $J^{\text{eff}}_{\text{Fe2}-\text{Fe3}}$ are very similar with 54.1 and 55.7 meV, respectively. Yet the individual differences with the FiM configuration are profound. Whereas $J^{\text{eff}}_{\text{Fe1}-\text{Fe2}}$ has an opposite sign, $J^{\text{eff}}_{\text{Fe2}-\text{Fe3}}$ is reduced by 56% between the FiM and FM configurations. Therefore, $Fe_3O_4^+$ exhibits strong non-Heisenberg behavior.

Furthermore, the optimized geometric structure of FM Fe3O4+ shows similar non-Heisenberg behavior to FiM Fe3O4+. Moreover, the difference in effective exchange interactions between these two structures is smaller than 4.3 meV.

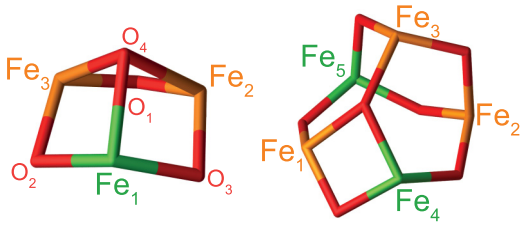

FIG. 2. The geometric structure of the $Fe_3O_4^+$ (left) and $Fe_5O_7^+$ (right) clusters. Orange and green indicate Fe atoms with ground state magnetic moments up and down, respectively. Red corresponds to O.

TABLE III. Effective exchange interactions of $Fe_5O_7^+$ for the FiM and FM configurations. All exchange interactions can be identified using Fig. 2.

	FiM (meV)	FM (meV)
$J^{eff}_{Fe1-Fe3}$	− 7.4	− 6.5
$J^{eff}_{Fe1-Fe4}$	− 39.7	38.2
$J^{eff}_{Fe1-Fe5}$	− 25.7	9.0
$J^{eff}_{Fe2-Fe3}$	71.4	17.2
$J^{eff}_{Fe2-Fe4}$	− 40.4	9.5
$J^{eff}_{Fe2-Fe5}$	− 56.9	10.7
$J^{eff}_{Fe3-Fe4}$	− 19.0	− 6.6
$J^{eff}_{Fe3-Fe5}$	− 62.1	13.0

Also larger cluster sizes show strong non-Heisenberg behavior as can be seen for $Fe_5O_7^+$ in Table III. All effective exchange interactions in the AFM ground state except $J^{eff}_{Fe2-Fe3}$ favor AFM ordering. $J^{eff}_{Fe2-Fe3} = 71.4$ meV corresponds to the single FM bond in the FiM ground state. In contrast to the exchange interactions in the FiM configuration, in the FM configuration the six largest exchange interactions favor FM order. Furthermore, J^{eff}_4 is reduced by 76% to 17.2 meV in the FM configuration compared to the FiM configuration. A similar reduction in strength between the FiM and FM interactions is observed for J^{eff}_3, J^{eff}_5, J^{eff}_6, and J^{eff}_8, which not only have an opposite sign but also are reduced by 65%, 76%, 81%, and 79%, respectively.

Figure 3 shows the individual and average effective exchange interactions for neutral and cation $Fe_xO_y^+$ clusters as a function of cluster size for both the FiM and FM configurations. Note that the difference between exchange interactions in the FM clusters is significantly reduced compared to the FiM configuration. This can be understood since all the oxygen atoms are similarly spin polarized in the FM configuration and every exchange interaction experiences approximately the same contribution due to spin polarization. Furthermore, note that on average the exchange interactions for the FiM configuration favor antiferromagnetic (AFM) alignment more compared to the FM exchange interactions.

Compared to bulk hematite, in clusters the exchange interactions are increased by an order of magnitude. With this, the interactions become strongly non-Heisenberg and are accompanied by a strong spin polarization of oxygen sites. It would be interesting to estimate the transition size where the cluster-to-bulk transition occurs. However, as the trend of the average effective exchange in Fig. 3 is not monotonous such an estimation requires *ab initio* calculations for larger cluster sizes and is beyond the scope of this Rapid Communication.

In bulk TM oxides super and double exchange mediate the indirect exchange interactions as direct TM-TM overlap is negligible. In the considered $Fe_3O_4^+$ and $Fe_5O_7^+$ clusters only trivalent Fe atoms are present as can be seen from Table I. Double exchange, often associated to strong non-Heisenberg behavior, requires different valence states between atoms and can therefore be excluded leaving superexchange as the dominant exchange mechanism. In superexchange, virtual hopping between the Fe $3d$ and O $2p$ levels is responsible for the magnetic order. Usually the energy involved is assumed to be small and considered a perturbation to the ionic picture [22]. In some cases however, such as cuprates, the covalency plays a more fundamental role, where the strong $3d$-$2p$ hybridization of Cu and O states results in unusually strong AFM exchange interactions [40–42]. In Heusler alloys, covalent magnetism is responsible for the observed non-Heisenberg behavior [43]. In clusters, hybridization effects play an important role even in determining their morphology [44,45]. We therefore calculate the hybridization index H_{dp}, which determines the overlap in DOS between the Fe-d and O-p orbitals:

$$H_{dp} = \frac{1}{N_e N_b} \sum_{i=1}^{N_e} \sum_{\substack{j \in \mathrm{Fe}, \\ k \in \mathrm{O}}} S\left(w^i_{d,j}, w^i_{p,k}\right), \tag{7}$$

where N_e and N_b are the number of bonds and number of electrons, respectively, j and k label the Fe and O sites, S is the overlap function, and $w^i_{l,j}$ is the sum of the projections of the ith Kohn-Sham orbital on the spherical harmonics $[Y^j_{l,m}(\mathbf{r})]$

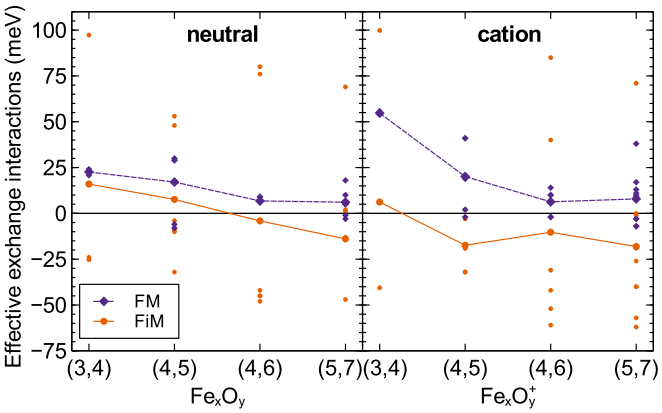

FIG. 3. The average (circles and lines) and individual (diamonds) effective exchange interactions for the neutral and cation Fe_xO_y clusters as a function of size (x, y).

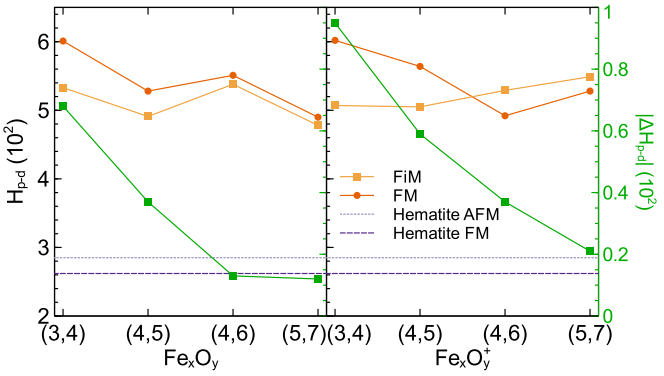

FIG. 4. The hybridization function (H_{dp}) as a function of cluster size for neutral and cation clusters and hematite. The absolute difference in hybridization between FM and FiM is shown in green as a function of cluster size.

at site j:

$$w^i_{l,j} = \sum_m \int |Y_{l,m}(\mathbf{r}_j)\phi_i(\mathbf{r})|^2 d\mathbf{r}. \quad (8)$$

The integration is performed within an atomic sphere with a radius of 1.32 Å and 0.82 Å for Fe and O, respectively.

Figure 4 shows H_{dp} as a function of cluster size for both the neutral and cation clusters. The purple dashed lines indicate the hybridization for AFM and FM hematite. Note that for clusters H_{dp} is twice as large compared to bulk hematite, and the hybridization difference between the FiM and FM configuration is more pronounced. Furthermore, the difference in hybridization between the FiM and FM configuration is significantly larger for smaller cluster sizes.

In covalent magnetism, molecular orbitals (MO) between atoms are considered as the source of magnetic order. As the occupation of a MO is inversely proportional to the energy difference of the MO and the atomic level, a shift in spectral weight occurs [46,47]. This is shown schematically in Fig. 5(a), where the length of the arrows indicates the contribution of spectral weight to that MO. Note that as the atomic O level is below the atomic Fe level, a ferromagnetic spin polarization on oxygen occurs. The MO's in Fig. 5(a) match very well with the projected DOS of the FM $Fe_3O_4^+$ cluster shown in Fig. 5(b), in full support of this picture.

As the hopping parameters t^σ_{ij} depend on the orbital overlap and hence hybridization, the difference in hybridization can therefore explain the observed changes in exchange interactions. We therefore attribute the strong non-Heisenberg behavior in these clusters to covalent magnetism, in particular to the change of hybridization between the Fe $3d$ and O $2p$ levels and oxygen spin polarization between different magnetic configurations.

In conclusion, we have shown that the magnetic moments of O in $Fe_xO_y^{0/+}$ clusters show unusually strong spin polarization depending on the magnetic configuration of the cluster compared to magnetite, where only moderate spin polarization in the FM configuration is observed. The exchange interactions in clusters show non-Heisenberg behavior and depend strongly on the magnetic configuration considered. The non-Heisenberg behavior is attributed to covalent magnetism since the hybridization between Fe $3d$ and O $2p$ orbitals for clusters is stronger than in hematite and depends on the magnetic configuration.

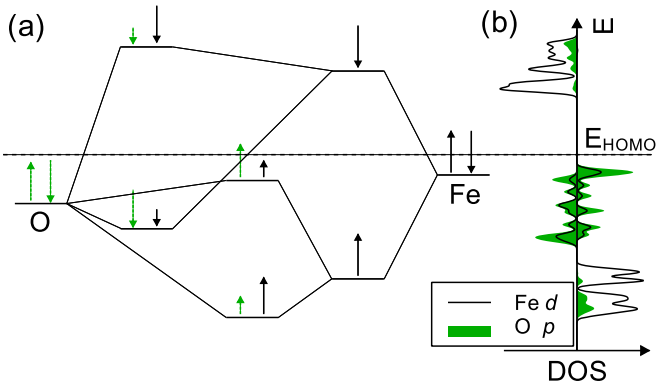

FIG. 5. A schematic MO diagram (a) between Fe and O. The arrows indicate the contribution of spectral weight to the MO. As the atomic O level is lower in energy than that of Fe, spin polarization on oxygen occurs. The projected DOS of the FM $Fe_3O_4^+$ cluster (b) where green corresponds to O p and black to Fe d.

We are thankful to V. V. Mazurenko and Y. O. Kvashnin for stimulating discussions. The Nederlandse Organisatie voor Wetenschappelijk Onderzoek (NWO) and SURFsara are acknowledged for the usage of the LISA supercomputer and their support. The work is supported by European Research Council (ERC) Advanced Grant No. 338957 FEMTO/NANO. A.N.R. acknowledges support from the Ministry of Education and Science of the Russian Federation, Project No. 3.7372.2017/BP.

[1] A. J. Cox, J. G. Louderback, and L. A. Bloomfield, Phys. Rev. Lett. **71**, 923 (1993).
[2] A. J. Cox, J. G. Louderback, S. E. Apsel, and L. A. Bloomfield, Phys. Rev. B **49**, 12295 (1994).
[3] M. B. Knickelbein, Phys. Rev. Lett. **86**, 5255 (2001).
[4] I. M. L. Billas, A. Châtelain, and W. A. de Heer, Science **265**, 1682 (1994).
[5] A. Langenberg, K. Hirsch, A. Ławicki, V. Zamudio-Bayer, M. Niemeyer, P. Chmiela, B. Langbehn, A. Terasaki, B. v. Issendorff, and J. T. Lau, Phys. Rev. B **90**, 184420 (2014).
[6] S. E. Apsel, J. W. Emmert, J. Deng, and L. A. Bloomfield, Phys. Rev. Lett. **76**, 1441 (1996).
[7] J. P. Bucher, D. C. Douglass, and L. A. Bloomfield, Phys. Rev. Lett. **66**, 3052 (1991).
[8] L. Peters, S. Ghosh, B. Sanyal, C. van Dijk, J. Bowlan, W. de Heer, A. Delin, I. Di Marco, O. Eriksson, M. I. Katsnelson, B. Johansson, and A. Kirilyuk, Sci. Rep. **6**, 19676 (2016).
[9] S. V. Vonsovsky, *Magnetism*, Vol. 2 (John Wiley and Sons, New York, 1974).
[10] C. Franchini, V. Bayer, R. Podloucky, J. Paier, and G. Kresse, Phys. Rev. B **72**, 045132 (2005).
[11] G. Fischer, M. Däne, A. Ernst, P. Bruno, M. Lüders, Z. Szotek, W. Temmerman, and W. Hergert, Phys. Rev. B **80**, 014408 (2009).
[12] A. Jacobsson, B. Sanyal, M. Ležaić, and S. Blügel, Phys. Rev. B **88**, 134427 (2013).
[13] D. M. Korotin, V. V. Mazurenko, V. I. Anisimov, and S. V. Streltsov, Phys. Rev. B **91**, 224405 (2015).
[14] Y. O. Kvashnin, O. Grånäs, I. Di Marco, M. I. Katsnelson, A. I. Lichtenstein, and O. Eriksson, Phys. Rev. B **91**, 125133 (2015).
[15] V. V. Mazurenko, Y. O. Kvashnin, F. Jin, H. A. De Raedt, A. I. Lichtenstein, and M. I. Katsnelson, Phys. Rev. B **89**, 214422 (2014).
[16] D. W. Boukhvalov, V. V. Dobrovitski, M. I. Katsnelson, A. I. Lichtenstein, B. N. Harmon, and P. Kögerler, Phys. Rev. B **70**, 054417 (2004).
[17] A. N. Rudenko, V. V. Mazurenko, V. I. Anisimov, and A. I. Lichtenstein, Phys. Rev. B **79**, 144418 (2009).

[18] R. Cardias, M. M. Bezerra-Neto, M. S. Ribeiro, A. Bergman, A. Szilva, O. Eriksson, and A. B. Klautau, Phys. Rev. B **93**, 014438 (2016).
[19] A. Bergman, L. Nordström, A. Burlamaqui Klautau, S. Frota-Pessôa, and O. Eriksson, Phys. Rev. B **75**, 224425 (2007).
[20] R. Logemann, G. A. de Wijs, M. I. Katsnelson, and A. Kirilyuk, Phys. Rev. B **92**, 144427 (2015).
[21] R. Logemann, A. N. Rudenko, M. I. Katsnelson, and A. Kirilyuk, J. Phys.: Condens. Matter **29**, 335801 (2017).
[22] P. W. Anderson, Phys. Rev. **115**, 2 (1959).
[23] Clarence Zener, Phys. Rev. **82**, 403 (1951).
[24] P. W. Anderson and H. Hasegawa, Phys. Rev. **100**, 675 (1955).
[25] A. D. Becke, J. Chem. Phys. **98**, 1372 (1993).
[26] We also checked LDA+U and obtained similar results.
[27] G. Kresse and J. Furthmüller, Phys. Rev. B **54**, 11169 (1996).
[28] P. E. Blöchl, Phys. Rev. B **50**, 17953 (1994).
[29] G. Kresse and D. Joubert, Phys. Rev. B **59**, 1758 (1999).
[30] A. A. Mostofi, J. R. Yates, Y. S. Lee, I. Souza, D. Vanderbilt, and N. Marzari, Comput. Phys. Commun. **178**, 685 (2008).
[31] See Supplemental Material at http://link.aps.org/supplemental/10.1103/PhysRevMaterials.2.073001 for atomic and magnetic moments of individual atoms, as well as for the exchange interactions.
[32] A. Erlebach, C. Hühn, R. Jana, and M. Sierka, Phys. Chem. Chem. Phys. **16**, 26421 (2014).
[33] A. I. Liechtenstein, M. I. Katsnelson, V. P. Antropov, and V. A. Gubanov, J. Magn. Magn. Mater. **67**, 65 (1987).
[34] M. Pajda, J. Kudrnovský, I. Turek, V. Drchal, and P. Bruno, Phys. Rev. B **64**, 174402 (2001).
[35] I. Turek, J. Kudrnovský, V. Drchal, and P. Bruno, Philos. Mag. **86**, 1713 (2006).
[36] M. I. Katsnelson, V. Y. Irkhin, L. Chioncel, A. I. Lichtenstein, and R. A. de Groot, Rev. Mod. Phys. **80**, 315 (2008).
[37] K. Sato, L. Bergqvist, J. Kudrnovský, P. H. Dederichs, O. Eriksson, I. Turek, B. Sanyal, G. Bouzerar, H. Katayama-Yoshida, V. A. Dinh, T. Fukushima, H. Kizaki, and R. Zeller, Rev. Mod. Phys. **82**, 1633 (2010).
[38] H. Ebert, D. Ködderitzsch, and J. Minár, Rep. Prog. Phys. **74**, 096501 (2011).
[39] A. N. Rudenko, F. J. Keil, M. I. Katsnelson, and A. I. Lichtenstein, Phys. Rev. B **88**, 081405(R) (2013).
[40] P. Bourges, H. Casalta, A. S. Ivanov, and D. Petitgrand, Phys. Rev. Lett. **79**, 4906 (1997).
[41] R. Coldea, S. M. Hayden, G. Aeppli, T. G. Perring, C. D. Frost, T. E. Mason, S. W. Cheong, and Z. Fisk, Phys. Rev. Lett. **86**, 5377 (2001).
[42] A. C. Walters, T. G. Perring, J.-S. Caux, A. T. Savici, G. D. Gu, C.-C. Lee, W. Ku, and I. A. Zaliznyak, Nat. Phys. **5**, 867 (2009).
[43] A. R. Williams, V. L. Moruzzi, C. D. Gelatt Jr., J. Kübler, and K. Schwarz, J. Appl. Phys. **53**, 2019 (1982).
[44] H. Häkkinen, M. Moseler, and U. Landman, Phys. Rev. Lett. **89**, 033401 (2002).
[45] S. Ganguly, M. Kabir, B. Sanyal, and A. Mookerjee, Phys. Rev. B **83**, 020411(R) (2011).
[46] A. R. Williams, R. Zeller, V. L. Moruzzi, C. D. Gelatt Jr., and J. Kubler, J. Appl. Phys. **52**, 2067 (1981).
[47] P. Mohn, *Magnetism in the Solid State An Introduction* (Springer-Verlag, Berlin, 2006).